resultant predicted by the shell bending theory is

$$Q_x = \frac{-Ic(\pi h/a)^{1/2}}{\Gamma(\frac{1}{4})}\left[\frac{2E_x(1-\nu_{x\theta}\nu_{\theta x})^{1/2}}{3E_{\theta}\tau}\right]^{1/4} \times J_{-1/4}[(1-\nu_{x\theta}\nu_{\theta x})^{1/2}\tau] \qquad (8)$$

where Γ is the gamma function and $J_{-1/4}$ is the Bessel function of the first kind of order $-\frac{1}{4}$. Q_x predicted by the shell bending theory has a singularity of the type $(\tau)^{-1/2}$ as $\tau \rightarrow 0$; whereas the Timoshenko-type shell theory predicts a finite value.

Discussion and Numerical Results

In view of Eq. (1c), there are four independent elastic constants for the orthotropic material. For the special case where $E_x = E_\theta = E$ and $\nu_{x\theta} = \nu_{\theta x} = \nu$, there are three independent elastic constants E, ν, G; this material is termed transversely isotropic. The bending stress at the outer surfaces of a shell with $a/h = 10$ predicted by both shell theories for a transversely isotropic material is shown in Fig. 1. The ratio $E/G = 2.6$ corresponds to the isotropic case for $\nu = 0.30$, and the values $E/G = 20$ and 50 correspond to pyrolytic graphite. These results indicate that the shell bending theory becomes less accurate for predicting maximum bending stresses as the E/G ratio increases and that the bending stresses are reduced as G is reduced. Results for an orthotropic material with $E_\theta/E_x = 10$ and $a/h = 10$ are presented in Fig. 2. These results indicate that the bending stresses are reduced as E_x is reduced.

The response of the shear stress resultant at the clamped support for a transversely isotropic material is presented in Fig. 3 for $a/h = 10$. The early time response is described by Eq. (7) and the remainder of the response is described by Eq. (8). Then the entire response can be closely approximated for the entire regime by piecing the two solutions together.

References

[1] Sagartz, M. J. and Forrestal, M. J., "Transient Stresses at a Clamped Support of a Circular Cylindrical Shell," *Journal of Applied Mechanics*, Vol. 36, No. 2, June 1969, pp. 367–369.

[2] Baker, E. H. and Herrmann, G., "Vibrations of Orthotropic Cylindrical Sandwich Shells under Initial Stress," *AIAA Journal*, Vol. 4, No. 6, June 1966, pp. 1063–1070.

[3] Kraus, H., *Thin Elastic Shells*, Wiley, New York, 1967.

Postbuckling Behavior of Geometrically Imperfect Composite Cylindrical Shells under Axial Compression

N. S. Khot*
Air Force Flight Dynamics Laboratory,
Wright-Patterson Air Force Base, Ohio

THIS Note is concerned with the influence of initial geometric imperfections on the buckling behavior of laminated anisotropic cylindrical shells. It has been established that the geometric imperfections reduce the buckling strength of isotropic cylindrical shells and the extent of the reduction has been studied intensively.[1,2] A similar reduction in buckling strength due to initial geometric imperfections may be expected in case of the anisotropic shells. In the present analysis von Kármán-Donnell large displacement relations, modified to include geometric imperfections are used. The solution to the problem is obtained by the application of the principle of stationary potential energy.

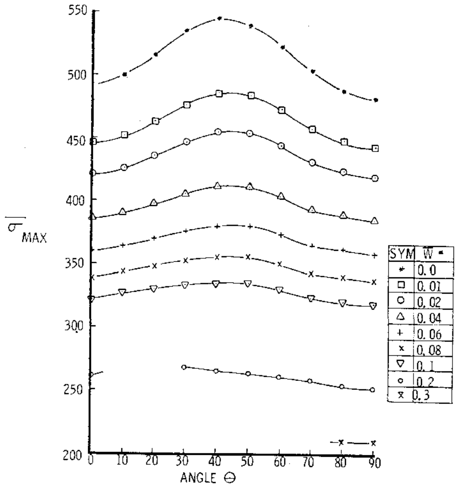

Fig. 1 Influence of initial imperfection on buckling load of three-layer, glass-epoxy composite cylinder for fiber orientation ($\theta°, -\theta°, 0°$).

Analytical Formulation

The relations between resultant stresses and strains for the laminated shell wall can be written as

$$[\epsilon] = [a][N] + [d]^T[k] \quad [M] = [d][N] - [d^*][k] \qquad (1)$$

where $[\epsilon]$, $[k]$ represent strains and changes of curvature while $[N]$ and $[M]$ are resultant stresses and moments. The definitions of matrices $[a]$, $[d]$, and $[d^*]$ may be found in Ref. 3.

The total strain energy of a multilayered cylindrical shell of radius R and length L can be expressed as the sum of the following two expressions:

$$\pi_1 = \frac{1}{2}\int_0^L \int_0^{2\pi R} [N]^T[a][N]dxdy$$
$$\pi_2 = \frac{1}{2}\int_0^L \int_0^{2\pi R} [K]^T[d^*][K]dxdy \qquad (2)$$

The energy associated with the work done by the uniformly applied compressive end load $\bar{\sigma}$ is given by

$$\pi_3 = L\int_0^{2\pi R} \{-\bar{\sigma}\}\, dy \int_0^L \bar{\mathcal{E}}dx \qquad (3)$$

where $\bar{\mathcal{E}}$ is the unit end shortening.

The total potential energy is then given by

$$\pi = \pi_1 + \pi_2 + \pi_3 \qquad (4)$$

The functions selected to represent the total radial displacement W and the initial imperfection $\overline{W}$ are given below:

$$W = W_1 \cos\frac{\pi x}{l_x}\cos\frac{\pi y}{l_y} + W_2\cos\frac{2\pi x}{l_x} + W_3\cos\frac{2\pi x}{l_x}\cos\frac{2\pi y}{l_y} + W_4\cos\frac{4\pi x}{l_x} + W_0$$
$$\overline{W} = \overline{W}_1 \cos\frac{\pi x}{l_x}\cos\frac{\pi y}{l_y} + \overline{W}_2\cos\frac{2\pi x}{l_x} + \overline{W}_3\cos\frac{2\pi x}{l_x}\cos\frac{2\pi y}{l_y} + \overline{W}_4\cos\frac{4\pi x}{l_x} \qquad (5)$$

where W_0 through W_4 are the unknown coefficients and $\overline{W}_1$

Presented as Paper 69-93 at the AIAA 7th Aerospace Sciences, Meeting, New York, January 20–22, 1969; submitted February 5, 1969; revision received October 10, 1969.

* Aerospace Engineer, Structures Division. Member AIAA.

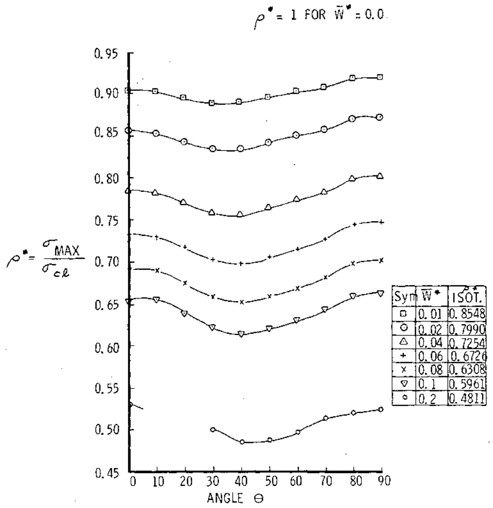

Fig. 2 Imperfection sensitivity of three-layer, glass-epoxy composite cylinder for fiber orientation ($\theta°$, $-\theta°$, $0°$).

through $\bar{W}_4$ are the amplitudes of the imperfection. l_x and l_y are the half-wave lengths in the axial and the circumferential directions.

Substitution of the expressions for W and $\bar{W}$ into the compatibility equation and subsequent solution would yield a compatible stress function which can be written as

$$F = \bar{F} - \bar{\sigma}y^2/2 \tag{6}$$

where $\bar{\sigma}$ is the applied axial compressive load and $\bar{F}$ is the trigonometric function consisting of eighteen terms.

Utilizing Eqs. (4–6) the algebraic expression for the total potential energy can be evaluated. The complete expression is given in Ref. 3. The energy expression contains ten stiffness parameters which are the functions of elements of matrices $[a]$, $[d]$ and, $[d^*]$ in Eq. (1). These can be evaluated knowing the dimensions of the shell and the elastic properties of the material in each layer of the laminated shell wall. The condition that for a given applied load, the total potential energy has a stationary value for small variations of the unknown displacement coefficients, gives nonlinear algebraic equations. These equations are solved of Newton-Raphson iterative technique.

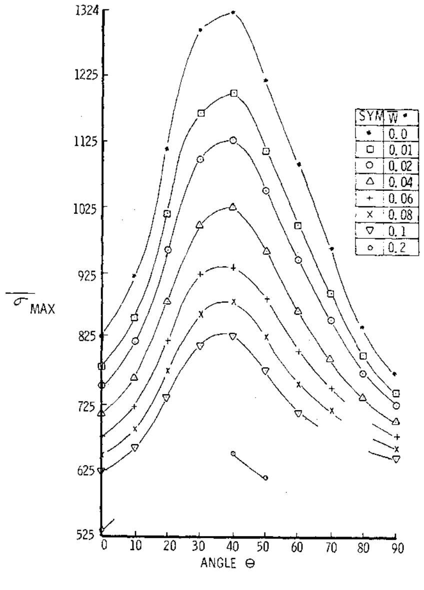

Fig. 3 Influence of initial imperfection on buckling load of three-layer, boron-epoxy composite cylinder for fiber orientation ($\theta°$, $-\theta°$, $0°$).

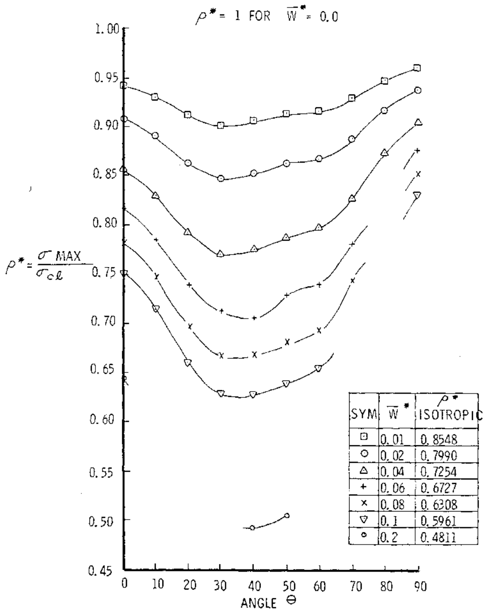

Fig. 4 Imperfection sensitivity of three-layer, boron-epoxy composite cylinder for fiber orientation ($\theta°$, $-\theta°$, $0°$).

The imperfection sensitivity of a cylindrical shell can be measured by a quantity ρ^* which is defined as the ratio of the buckling load of an initially imperfect shell $\bar{\sigma}_{\max}$ to the classical buckling load $\bar{\sigma}_{cl}$. For the perfect shell $\bar{\sigma}_{\max} = \bar{\sigma}_{cl}$ and ρ^* is equal to unity. To study the influence of initial geometric imperfections the relative values of the initial imperfection amplitudes are assumed to be

$$\bar{W}_1 = 4\bar{W}_2 = -4\bar{W}_3 = 16\bar{W}_4 \tag{7}$$

These values correspond to the Yoshimura buckling pattern.[2] The imperfection parameter $\bar{W}^*$ is defined here as the ratio of the sum of initial imperfection amplitudes to the total thickness of the shell. The wavelengths of the initial imperfection are assumed to be the same as those of small deflection buckling load. For anisotropic shell the buckling load and the corresponding buckling mode for small deflection theory are calculated from equations given in Ref. 4.

Numerical Results

As mentioned before, the behavior of the shell depends upon ten stiffness parameters. As an example, a three-layer cylindrical shell of 6.0-in. radius and 0.036-in. thickness is selected to present the results. The thickness of each layer is 0.012 in. and all layers consist of either glass-epoxy or boron-epoxy composites. The elastic constants for glass-epoxy composites are: $E_{11} = 7.5 \times 10^6$ psi; $E_{22} = 3.5 \times 10^6$ psi; $\nu_{12} = 0.25$; $G = 1.25 \times 10^6$ psi. And for boron-epoxy the constants are: $E_{11} = 40.0 \times 10^6$ psi; $E_{22} = 4.5 \times 10^6$ psi; $\nu_{12} = 0.25$; $G = 1.5 \times 10^6$ psi. The results are presented here for one set of fiber orientations. The fiber orientations in outer, middle, and inner layers are $\theta°$, $-\theta°$, $0°$ respectively. θ assumes values ranging from 0° to 90° with ten degrees interval. When θ is zero, fibers are axially oriented, and when it is 90° the fibers are circumferentially oriented.

The values of $\bar{\sigma}_{\max}$ and ρ^* for various fiber orientations and for different values of the imperfection parameter $\bar{W}^*$ are presented in Figs. 1–4. The discontinuity in the curves indicates that for that range of fiber orientation there is no snap-buckling observed on the load-shortening curves. Evidently, this is because the four-term expression selected to represent the radial displacement function W is not sufficient. In order to find snap-buckling load for larger values of $\bar{W}^*$, it may be necessary to use a more complete expression for W than the one used in Eq. (5). Figure 1 gives the variation of $\bar{\sigma}_{\max}$ with the fiber orientation for glass-epoxy composite shell. Figure 2 shows the variation of imperfection sensitivity ρ^* for the same set. From these two figures, it is seen that increase or decrease in classical buckling load with change in fiber orientation is generally accompanied by a decrease or increase in imperfection sensitivity. The same behavior can be observed for boron-epoxy composite shell from Figs. 3 and 4. In Figs. 2 and 4, the values of ρ^* for isotropic shell are given for the purpose of comparison. It can be seen that the composite shells are less imperfection sensitive than isotropic shells and boron-epoxy composite shells are less imperfection sensitive than glass-epoxy shells.

References

[1] Donnell, L. H. and Wan, C., "Effect of Imperfections on Buckling of Thin Cylinders and Columns under Axial Compression," *Journal of Applied Mechanics*, Vol. 17, No. 1, 1950, p. 73.

[2] Madsen, W. A. and Hoff, N. J., "The Snap-Through and Postbuckling Equilibrium Behavior of Circular Shells Under Axial Load," SUDAER 227, 1965, Stanford Univ.

[3] Khot, N. S., "On the Influence of Initial Geometric Imperfections on the Buckling and Postbuckling Behavior of Fiber-Reinforced Cylindrical Shells under Uniform Axial Compression," TR-68-136, 1968, Air Force Flight Dynamics Lab., Wright-Patterson Air Force Base, Ohio.

[4] Khot, N. S., "Buckling and Postbuckling Behavior of Composite Cylindrical Shells under Axial Compression," *AIAA Journal*, Vol. 8, No. 2, Feb. 1970, pp. 229–235.

Laser Holographic Interferometry Study of High-Speed Flowfields

A. B. Witte* and R. F. Wuerker†
TRW Inc., Redondo Beach, Calif.

It is the purpose of this Note to show examples of pulsed laser holographic interferograms of 40° viewing angle recorded in a small ballistic range having a 6-in. scene depth (early results in a large range having a 6-ft scene depth are reported elsewhere[1]); and to demonstrate that data reduction of the fringe pattern can be accomplished to obtain quantitative density field about high-speed projectiles.

Photographs of the holographic interferogram of the shock-on-shock interaction, shown in Figs. 1–3, comprise the intersection of a 22 caliber 60° cone-cylinder projectile fired at free-stream Mach number, M, of 3.4 at NTP and a weak spherical shock wave ($M = 1.1$) created by a spark gap discharge of a capacitor. A detailed description of the holograph technique used to produce these results is contained in Refs. 1 and 2. The three views taken at $-20°$, $0°$, and $20°$ define a continuous viewing angle of about 40° from this single holographic interferogram and demonstrate the three-dimensional properties of the holographic interferogram as can be seen readily at the intersection of the two shock waves as one looks from view to view. It is doubtful that Mach Zehnder interferometry will ever be capable of such versatility. In Ref. 1, a discussion is given of the prospects of utilizing these multiple views to accomplish three-dimensional data reduction of complicated flowfields.

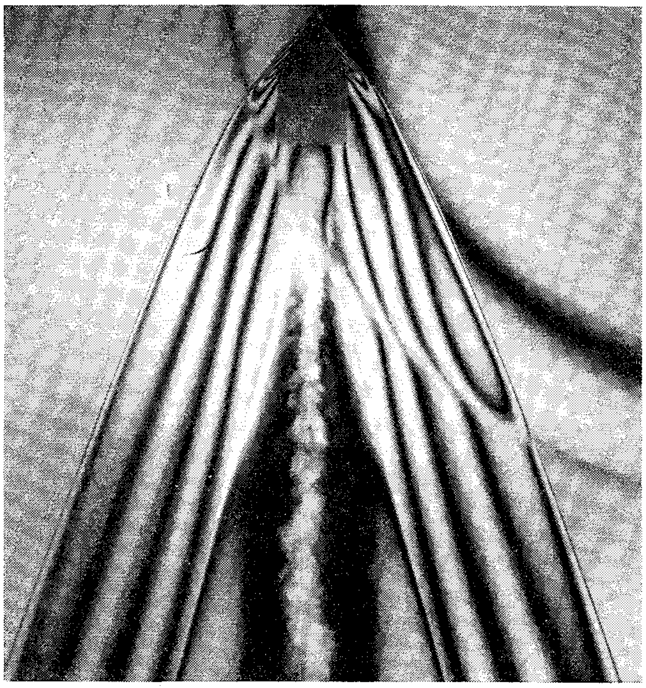

Fig. 1 Interferogram of projectile-blast wave interaction: −20° view.

The holographic interferogram of the tip of a projectile fired in Xenon, shown in Fig. 4, was recorded and reported earlier by Heflinger, Wuerker, and Brooks of this Laboratory.[2] The dots on or near the experimental fringe pattern were calculated values of fringe location based upon a constant density model of the flowfield behind the shock wave.[2] The agreement between their experiment and flow model is good.

The calculation of density field from fringe pattern, which is normally done in interferometry by the aerodynamicist, is now demonstrated for the projectile in Fig. 4. For purposes of data reduction, the standard equation for fringe shift was inverted by the Abel integral, which in turn was expressed in finite difference form as described in detail in Ref. 1. The

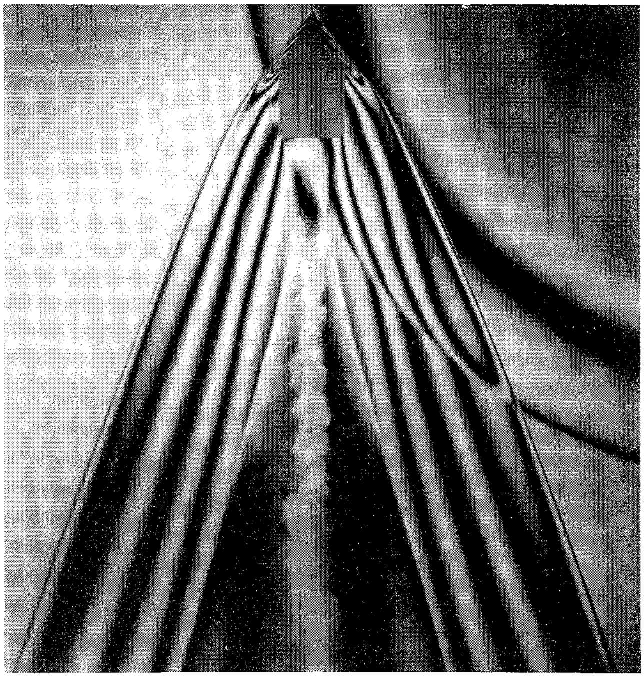

Fig. 2 Interferogram of projectile-blast wave interaction: 0° view.

Presented as Paper 69-347 at the AIAA 4th Aerodynamic Testing Conference, Cincinnati, Ohio, April 28–30, 1969; submitted May 15, 1969; revision received September 29, 1969. This research was supported by the Advanced Research Projects Agency of the Department of Defense and was monitored by NIKE Development Office, DAHC 60-69-C-0006.

* Head Experimental Staff, Fluid Mechanics Laboratory. Associate Member AIAA.

† Senior Scientist, Physical Electronics Laboratory.